

# Neuromedin C: Potential-Dependent Surface-Enhanced Raman Spectra in the Far-Red Spectral Region on Silver, Gold, and Copper Surfaces

Edyta Podstawka-Proniewicz,<sup>\*†</sup> Gediminas Niaura,<sup>‡</sup> and Leonard M. Proniewicz<sup>†</sup>

Faculty of Chemistry, Jagiellonian University, ul. Ingardena 3, 30-060 Krakow, Poland,

Department of Bioelectrochemistry and Biospectroscopy, Institute of Biochemistry, Mokslininkų 12, LT-08662 Vilnius, Lithuania

Received: November 5, 2009; Revised Manuscript Received: February 23, 2010

Neuromedin C (NMC) is a decapeptide (Gly-Asn-His-Trp-Ala-Val-Gly-His-Leu-Met-NH<sub>2</sub>) that acts as a growth factor in a wide range of tumors including carcinomas of the pancreas, stomach, breast, prostate, and colon. We report surface-enhanced Raman spectra (SERS) of NMC on electrochemically roughened Ag, Au, and Cu electrode surfaces over an electrode potential range varying from +0.200 to -1.200 V (depending on the electrode material). We compared the SERS spectra to the Raman spectrum of the corresponding solid species. The SERS spectra were dominated by L-tryptophan (Trp) vibrations. This indicates that Trp interacted with the metallic surfaces of the electrodes, either by binding directly to the surface or by staying in close proximity to the surface. Characteristic SERS bands showed that, in the case of the Ag electrode, the Trp residue was almost perpendicular to the surface. In contrast, the Trp residue was slightly tilted with respect to the Au electrode surface, and Trp remained some distance from the surface of the Cu electrode. These differences were due to differences in surface rheology and in the type of metal (Ag vs Au vs Cu) responsible for the observed enhancement mechanism. On the other hand, variations in the electrode potentials only had a slight influence on the SERS patterns and the observed changes were mainly due to the reorientation of the Trp ring with respect to the electrode surface. These findings were fully supported by generalized two-dimensional correlation analysis (G2DCA).

## Introduction

The mammalian homologue of bombesin (BN) is gastrin-releasing peptide (GRP), which can be isolated from the gastric tissues of pigs and other mammals.<sup>1–3</sup> GRP is known to be widely distributed throughout the gastrointestinal tract and central nervous system.<sup>4,5</sup> The active fragment of GRP, neuromedin C (GRP18–27, NMC, or [His7]BN5–14; Gly-Asn-His-Trp-Ala-Val-Gly-His-Leu-Met-NH<sub>2</sub>), has a C-terminal amino acid sequence from the fifth to the 14th position that is similar to BN. This similarity is responsible for the related pharmacological effects of the two species.<sup>6–8</sup>

Previously, within this biological context, we evaluated the molecular structures of NMC and related peptides in the solid state and then defined their ordered superstructures on colloidal and electrochemically roughened Ag substrates in aqueous solution.<sup>9,10</sup> The use of an aqueous solution and these two types of Ag substrates provided new insight into the surface phenomena governing NMC under physiological conditions (measurements were done over a pH range of 7.0–8.3). The establishment of the SERS technique in chemical analysis has allowed for the study of adsorption processes in various samples by observing characteristic vibrational bands for certain functional groups.<sup>11</sup> The nature of this technique, along with its chemical specificity, makes it ideally suited to elucidate molecular structures of adsorbed species, surface processes, and interface reactions.<sup>12,13</sup> This technique has been successfully employed to study many biological systems, including peptide

interactions, protein folding, and diseased tissues.<sup>14–16</sup> SERS is also useful in modeling ligand–receptor binding for drug–protein screening.<sup>17,18</sup> Therefore, in the present work we focused on electrode surfaces made of roughened Ag, Au, and Cu. We aimed to investigate potential-dependent NMC…Ag, NMC…Au, and NMC…Cu interactions to further facilitate the understanding of the physiological function of NMC. We also aimed to explore opportunities for therapeutic intervention using NMC. Further changes in selectivity might be triggered by the electrode potential and by the nature of the electrode.

To better understand the issues described above, we characterized changes in band enhancement, broadness, and wave-number arising from the single amino acids or from fragments of the adsorbed peptides as a function of the type of metal substrate and the applied electrode potential. In this way, we provided some of the missing structural information concerning the chemisorption of NMC on roughened metal electrode surfaces. Generalized two-dimensional correlation analysis, which emphasizes spectral features not readily observed in conventional one-dimensional spectra, was used for detailed analysis of slight changes in SERS spectral signals as a function of the electrode potential. Such changes are typically due to minor alterations in the molecular geometry of the adsorbed species with respect to the substrate.

## Experimental Procedures

**Neurotransmitter.** Neuromedin C (NMC, GRP18–27, i.e., a fragment from the 18th to the 27th amino acid of gastrin releasing peptide) was purchased from Bachem Co., Switzerland. Its purity and chemical structure were verified by taking <sup>1</sup>H and <sup>13</sup>C NMR spectra (using a Bruker Avance DRX 300 MHz

\* Corresponding author. E-mail: podstawk@chemia.uj.edu.pl. Phone: +48-12-663-2077. Fax: +48-12-634-0515.

† Jagiellonian University.

‡ Institute of Biochemistry.

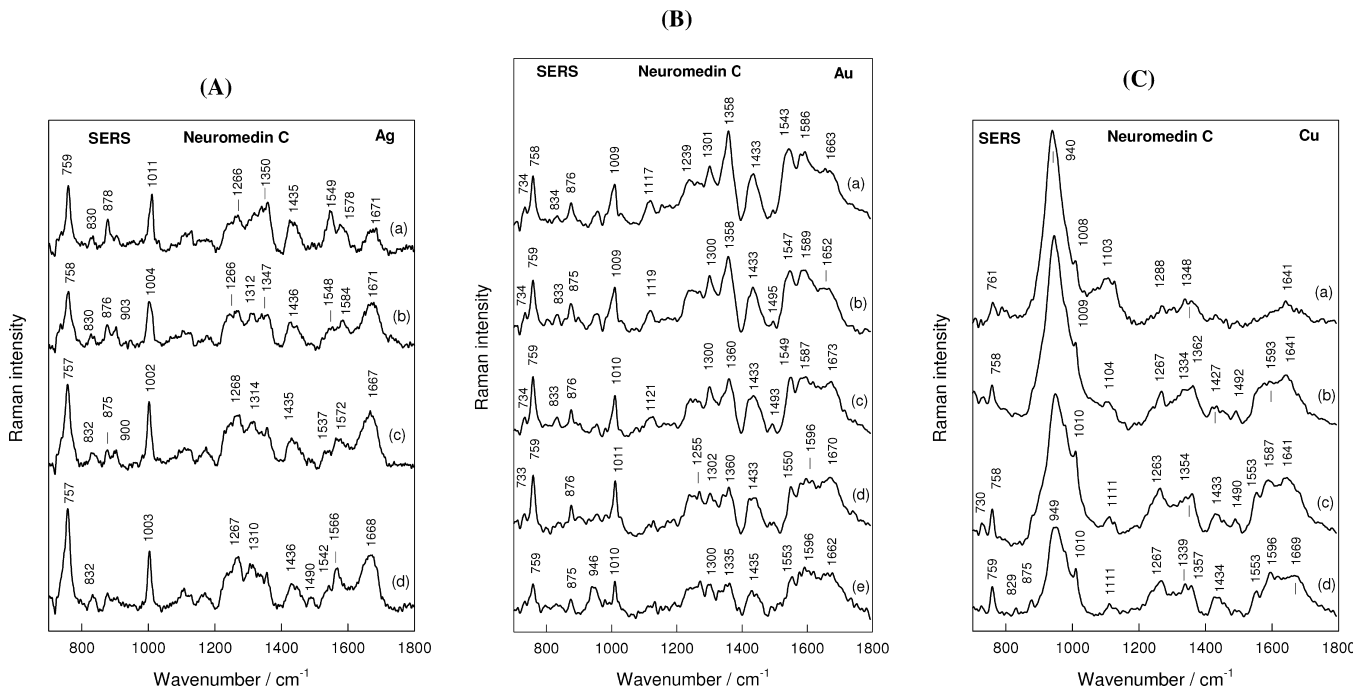


**Figure 1.** SERS spectra of Neuromedin C adsorbed on (A) a roughened Ag electrode at potentials of 0.000 V (a),  $-0.400$  V (b),  $-0.800$  V (c), and  $-1.200$  V (d); (B) a roughened Au electrode at potentials of  $+0.200$  V (a),  $+0.000$  V (b),  $-0.400$  V (c),  $-0.800$  V (d), and  $-1.200$  V (e); and (C) a roughened Cu electrode at potentials of  $-0.400$  V (a),  $-0.600$  V (b),  $-0.800$  V (c), and  $-1.200$  V (d). Measurements were taken in a 0.1 M  $\text{Na}_2\text{SO}_4$  solution containing 0.01 M phosphate buffer (pH 7.0) and  $10^{-5}$  M NMC. An excitation wavelength of 1064 nm and a laser power of 300 mW at the sample were used.

spectrometer) and by electrospray mass spectrometry (with a Finnigan Mat TSQ 700).

**SERS Measurements.** FT-SERS spectroscopic measurements were carried out using a Perkin-Elmer Model Spectrum GX FT-Raman spectrometer equipped with an InGaAs detector operating at room temperature. An air-cooled diode-pumped Nd: YAG laser with an emission wavelength of 1064 nm was used as the excitation source. In general, the laser power at the sample was 300 mW. The laser beam was focused to a spot of approximately  $1 \text{ mm}^2$  in area. Spectroelectrochemical measurements were carried out in a cylinder-shaped three-electrode moving cell, arranged with a flat circular electrode (gold, silver, or copper) of approximately 5 mm in diameter press-fitted into a Teflon rod, which served as the working electrode. Platinum wire was used as the counter electrode, and a KCl saturated Ag/AgCl electrode was used as the reference. All potential values reported in this work were taken with respect to this reference electrode. During the experiment, ultrapure Ar gas was continuously bubbled through the solution to remove dissolved oxygen. The working electrode was placed approximately 1 mm from the cell window. To reduce confounding effects from light and heat, the cell, together with the electrodes, was moved linearly with respect to the laser beam at a rate of about 15–25 mm/s.<sup>19,20</sup> Spectral resolution was set at  $4 \text{ cm}^{-1}$ , and the wavenumber increment per data point was  $1 \text{ cm}^{-1}$ . To enhance the signal-to-noise ratio, 200–400 scans were combined. The SERS spectra were measured from 3–4 samples and showed reproducible results (see Figure 1S in the Supporting Information).

Raman spectra of solid samples were recorded with a LabRam HR800 spectrometer (Horiba Jobin Yvon) equipped with a grating containing 600 grooves/mm. The 632.8 nm emission of a Spectra Physics He–Ne laser was used as the excitation source. The laser power at the sample was set to 10 mW. Raman spectra were taken using a  $50\times/0.50$  NA objective lens with a long working distance.

The Au electrodes for SERS were electrochemically roughened by potential scanning using a method similar to one reported previously.<sup>21,22</sup> Electrodes were scanned for 50 cycles in 0.1 M aqueous KCl using voltages between  $-0.300$  and  $+1.31$  V at a scan rate of 300 mV. Electrochemical roughening of the Ag and Cu electrodes was performed according to established methods as described in refs 23 and 24, respectively. Millipore purified ( $18.2 \text{ M}\Omega \text{ cm}$ ) water was used throughout the work.

**Generalized Two-Dimensional Correlation Analysis.** Generalized two-dimensional correlation analysis (G2DCA) of the SERS spectra of NMC adsorbed on the roughened Ag, Au, and Cu electrode surfaces was performed using 2Dshige version 1.3 software, written by Shigeaki Morita, Kwansei-Gakuin University, 2004–2005. Typically, the four potential-dependent SERS spectra of NMC were normalized. In the G2D correlation maps, regions colored by red indicate positive correlation intensities, while blue regions indicate negative correlation intensities.

## Results and Discussion

Figure 1 presents the SERS spectra of NMC adsorbed on (A) Ag, (B) Au, and (C) Cu electrode surfaces over electrode potentials ranging from  $+0.200$  to  $-1.200$  V. In all cases, spectra were obtained using a continuous Nd<sup>3+</sup>:YAG laser with a wavelength of 1064 nm. For comparison, the Raman spectrum of NMC in the solid state is shown in Figure 2. Detailed assignments of the Raman bands of NMC have been made previously.<sup>10</sup> In general, the SERS spectral patterns of NMC on Ag, Au, and Cu electrode surfaces, including band intensities and widths, were different from the Raman spectra (Figure 2)<sup>10</sup> and from the corresponding SERS spectra of this peptide in a silver sol.<sup>9</sup> This is not surprising, as the surface roughness present when using the SERS technique induces strong electromagnetic fields. This is most prevalent when unevenness such as that created by needle or nanostructure clusters is also present.<sup>25</sup> These fields act directly on the molecules adsorbed

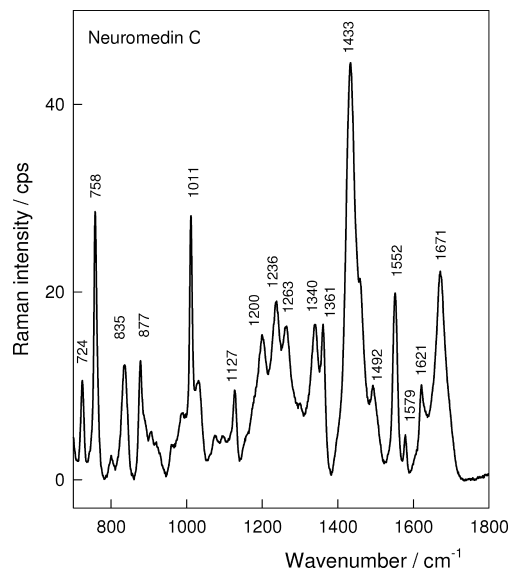


**Figure 2.** Raman spectrum of solid NMC, taken using an excitation wavelength of 632.8 nm and a laser power of 10 mW at the sample.

on the metal surface, increasing the intensity of the entire electromagnetic field as observed by the adsorbed molecule. Therefore, the structure of the monolayer of the adsorbed species and the relative strength of adsorption versus other interactions among the functional groups of the adsorbate strongly depend upon the roughness of the metal surface. Additionally, the properties of the adsorbed molecules and their response to electrical stimuli depend on the pH of the solution (via the formation of anionic, zwitterionic, or cationic species) and on the charge on the metal surfaces.

The SERS spectra of adsorbed NMC on different metal surfaces (Figure 1) contain similar sets of bands. Some distinct differences in the enhancement of individual bands can be clearly observed among these spectra. For instance, the most intense bands in the SERS spectra on Ag, at 759 and 1011 cm<sup>-1</sup> (Figure 1A), which are characteristic of indole ring interactions with the Ag electrode - were less enhanced on Au and Cu. Meanwhile, spectral features at 1358 and 1543 cm<sup>-1</sup> were more strongly enhanced on Au (Figure 1B) than on the other two substrates. These features are indicative of a favorable C<sub>3</sub>=C<sub>2</sub>—N<sub>1</sub>—C<sub>8</sub>...Au interaction (see Figure 3 for the atomic numbering scheme used for the Trp residue). One other noteworthy point is that a very strong spectral feature appeared around 940 cm<sup>-1</sup>, due to phosphate anions adsorbed at the Cu electrode (Figure 1C). Assignment of spectral bands was facilitated considerably by comparing SERS spectra recorded in H<sub>2</sub>O with those recorded in D<sub>2</sub>O (Figure 4). For example, the amide I mode at 1668 cm<sup>-1</sup> could be clearly recognized from the downward shift of this band in D<sub>2</sub>O due to amide group H/D exchange. Similarly, the amide III mode must be assigned to the 1265 cm<sup>-1</sup> SERS signal, since it disappeared in D<sub>2</sub>O. Indole ring modes were also clearly assignable (759/754, 878/856, 1431/1383, and 1491/1481 cm<sup>-1</sup>) as they were sensitive to H/D exchange at the N<sub>1</sub>—H site (Figure 4).

Assignment of the predominant SERS bands to normal coordinates was guided by previous data. Studies of the SERS spectra of NMC adsorbed on colloidal Ag nanoparticles,<sup>9</sup> of NMC on electrochemically roughened Ag substrates,<sup>10</sup> and of BN and related peptides deposited onto colloidal and electrode surfaces of Ag, Au, and Cu<sup>26–32</sup> were used. The in-phase indole ring breathing vibration (W18) was assigned to the band at 759 cm<sup>-1</sup>. The feature at 1011 cm<sup>-1</sup> was assigned to the out-of-

phase indole breathing vibration (W16). The SERS signals at 1358 and 1543 cm<sup>-1</sup> corresponded to pyrrole ring N<sub>1</sub>—C<sub>8</sub> stretching (W7) and pyrrole C<sub>2</sub>=C<sub>3</sub> stretching (W3), respectively. Additionally, the bands at ~832 cm<sup>-1</sup> ( $\nu$ (C—C) and  $\nu$ (C—N—C) of secondary amide), ~878 cm<sup>-1</sup> (W17;  $\delta$ (N<sub>1</sub>—H) + FR), 1266–1268 cm<sup>-1</sup> (amide III), ~1310 cm<sup>-1</sup> (W8;  $\nu$ (C<sub>3</sub>—C<sub>9</sub>) +  $\delta$ (N<sub>1</sub>—H)), 1435 cm<sup>-1</sup> (W6; pyrrole ( $\nu$ <sub>s</sub>(N<sub>1</sub>—C<sub>2</sub>=C<sub>3</sub>) +  $\delta$ (N<sub>1</sub>—H)), 1566–1578 cm<sup>-1</sup> (W2; phenyl), and 1667–1671 cm<sup>-1</sup> (amide I) (see Table 1 for detailed band positions) matched previously assigned Trp residue and —CONH— bond spectral features. Several bands contain contribution from His residues. First of all, this refers to the relatively strong and broad feature in the vicinity of 1572–1578 cm<sup>-1</sup>.<sup>33–35</sup> While the position of this band coincides with the W2 mode of the Trp residue, the intensity of the latter band usually is low. Two bands near 1347–1350 and 1310–1314 cm<sup>-1</sup> also contain a high contribution from His ring vibrations.<sup>33,34</sup> Finally, the broad feature at 1266–1268 cm<sup>-1</sup>, which is mainly associated with the amide III vibrational mode, we suppose, also has some contribution from imidazole ring vibration. The intense band at 1002–1004 cm<sup>-1</sup> we assigned to the perturbed vibrational mode of the indole ring of the Trp residue (W16). However, this band might have a small contribution from the His ring C—H in-plane bending mode.<sup>33,34</sup>

**Ag Electrode Surface.** By comparing the spectral profiles in Figure 1A, we observed small changes in the enhancement of the indole ring vibrations of Trp due to changes in the applied electrode potential. These variations were the result of subtle changes in molecular geometry relative to the Ag electrode surface. The orientation of the indole molecule and its substituted analogs on different metal surfaces has been widely investigated. For example, two adsorption modes have been predicted for N-containing heterocycles on a metal surface.<sup>35</sup> These modes include edge-on adsorption (through the lone electron pair on the nitrogen atom) and flat-on adsorption (through the  $\pi$ -electron system of the ring). Briefly, in the edge-on orientation, vibrational modes that are out-of-plane were either not present or weakly enhanced relative to the in-plane modes of the adsorbate. The ring breathing vibrations of the adsorbate usually increase in relative intensity upon adsorption, and the wavenumbers for most bands decrease. If flat-on adsorption, which is relatively weak, occurs, the wavenumbers of the modes associated with the ring decrease upon adsorption at more positive potentials, whereas the wavenumbers of the breathing modes generally increase as the potential becomes more negative.

Since the adsorption orientation was discernible by studying the aforementioned bands, we focused on analysis of these bands. The parameters of the W16 band (at ~1011 cm<sup>-1</sup>) in the SERS spectra of NMC on Ag (Figure 1A) depend on the electrode potential. The W18 and W16 indole ring modes (see Table 1 for band assignments) in the SERS spectra (Figure 1A) exhibited lower band intensities and higher band widths at half-maximum (fwhm = 17–24 cm<sup>-1</sup>) compared with similarly assigned bands in the corresponding Raman spectrum (fwhm = 10 cm<sup>-1</sup>) (Figure 2). In addition, the W18 band intensity increased and it broadened when the electrode potential became more negative (i.e., for W18 at 0.000 V, fwhm = 17 cm<sup>-1</sup> but this broadened to fwhm = 24 cm<sup>-1</sup> at –1.200 V). The same broadening also occurred for the W7 and W3 modes. However, the band positions of these spectral features did not change markedly ( $\Delta\nu$  = 0–11 cm<sup>-1</sup>). Lowering of W16 band frequency at more negative potentials (1002–1004 cm<sup>-1</sup>) indicates interaction of indole ring with the Ag surface. The amide I (1663–1671

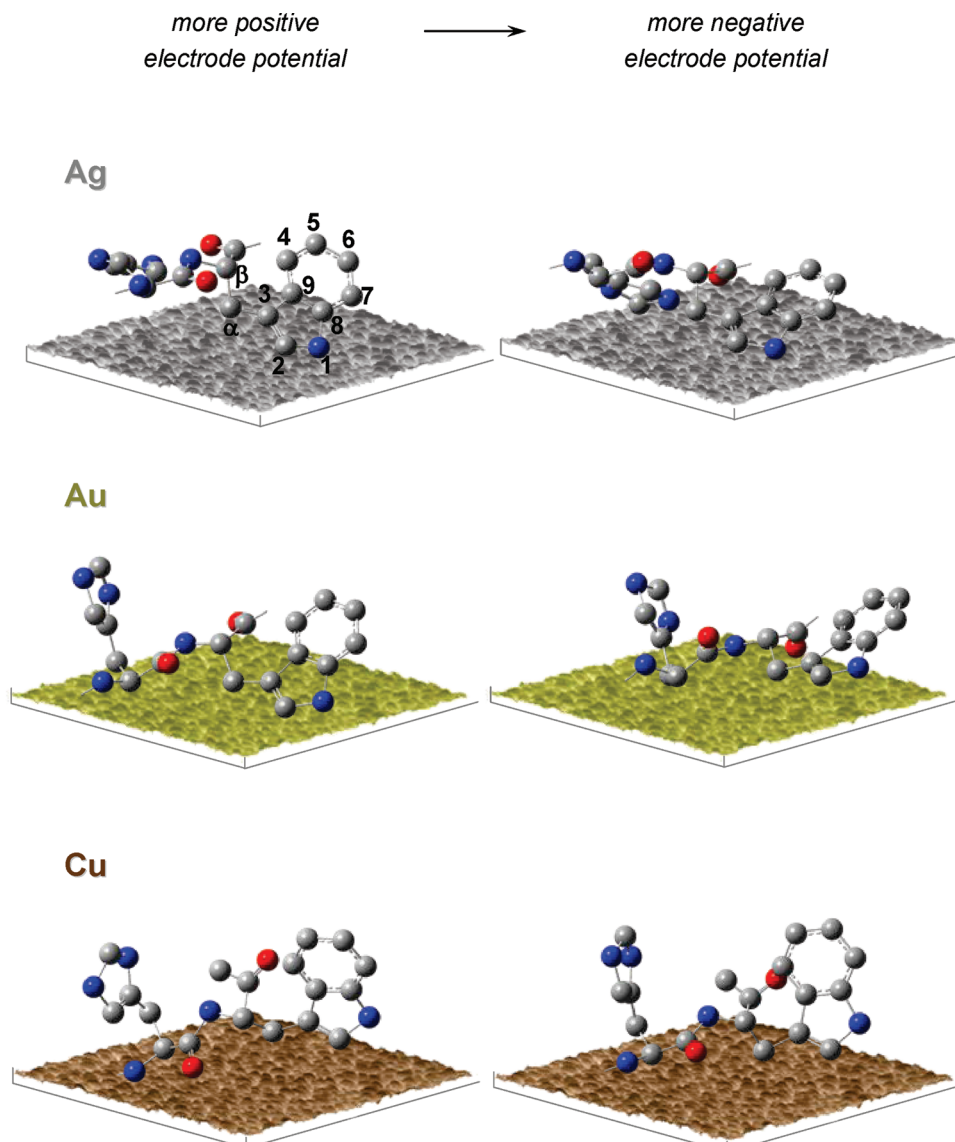


**Figure 3.** Possible manner of changes in the binding of the His3-CONH-Trp4 fragment of NMC to roughened Ag, Au, and Cu electrode surfaces together with the atomic numbering scheme for the tryptophan residue. Color scheme: blue, nitrogen; red, oxygen; gray, carbon atoms.

$\text{cm}^{-1}$ ) and III ( $\sim 1267 \text{ cm}^{-1}$ ; the presence of the AIII band around this wavenumber was visible from the spectral feature at  $1070 \text{ cm}^{-1}$  in  $\text{D}_2\text{O}$  as shown in Figure 4) SERS signals increased in intensity with decreasing electrode potential. The relative intensity of the bands containing contribution from His ring vibrations changes in different ways as the potential becomes more negative. The relative intensity of the  $1266 \text{ cm}^{-1}$  band increases, while the intensity of the  $1350$  and  $1578 \text{ cm}^{-1}$  spectral features decreases. These perturbations indicate reorientation of the His ring. The  $\pi$  overlap between the indole ring and the surface was higher at more negative electrode potentials. Furthermore, the interaction between Ag and the lone pair on the nitrogen atom of His was also more effective for more negative electrode potentials. Hence, we propose that on the Ag electrode surface at  $0.000 \text{ V}$ : (i) the indole ring was tilted with respect to the Ag surface and interacted with this surface mainly through the  $\text{C}_3=\text{C}_2-\text{N}_1-\text{C}_8$  fragment; (ii) the His residue lay nearly flat on this surface; and (iii) the amide bond remained in close proximity to this surface and was also nearly horizontal to this surface.

When the electrode potential became less positive, the indole ring moved slightly away from the surface normal. The phenyl

coring interacted slightly more with the electrode surface, and the pyrrole coring interacted slightly less. His, in its tilted orientation, interacted with Ag through both the N-H unit and the imidazole ring. Moreover, when the electrode potential became more negative, the angle formed between the amide bond and the surface increased, but the strength of the indirect amide bond $\cdots$ Ag electrode interaction remained almost unchanged. Because the changes observed in the SERS spectra correspond to the reorientation of the His, Trp, and  $-\text{CONH}-$  moieties on the Ag surface, the data imply that these units belong to the  $-\text{His3-CONH-Trp4-}$  fragment in the NMC amino acid sequence.

The differences described above are supported by G2D correlation maps. These maps are generally useful in the analysis of spectral signals that change slightly as a function of many kinds of physical variables, such as potential, that affect the spectra.<sup>26,36</sup> Figure 5A presents synchronous (left) and asynchronous (right) G2D correlation maps over the wavenumber range of  $1750$ – $600 \text{ cm}^{-1}$ , generated from the potential-dependent SERS spectra of NMC adsorbed on an Ag electrode surface. The synchronous G2D correlation map contains seven autopeaks, one with strong intensity (at  $(1671, 1671) \text{ cm}^{-1}$ ,

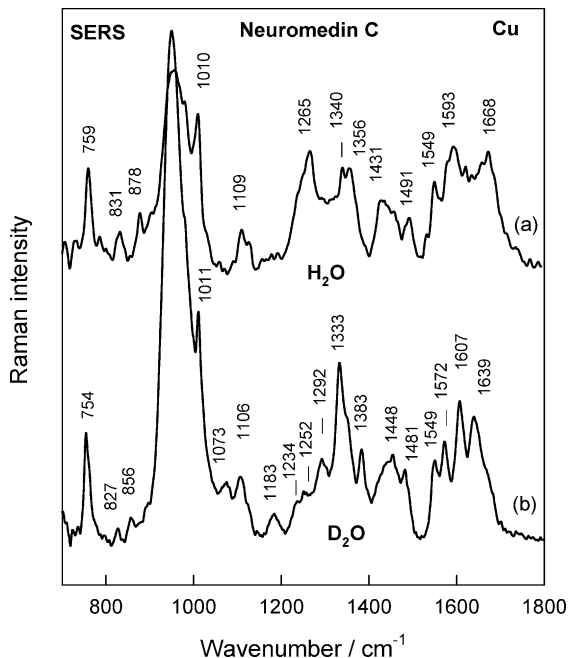


**Figure 4.** SERS spectra of NMC adsorbed on a roughened Cu electrode at  $-0.800$  V in solutions prepared with  $\text{H}_2\text{O}$  (a) and  $\text{D}_2\text{O}$  (b). Measurements were taken in a  $0.1$  M  $\text{Na}_2\text{SO}_4$  solution containing  $0.01$  M phosphate buffer (pH 7.0) and  $10^{-5}$  M NMC. Spectra were recorded after three potential cycles between  $-0.400$  and  $+1.200$  V, by keeping the electrode for 10 min at each potential. An excitation wavelength of  $1064$  nm and a laser power of  $300$  mW at the sample were used.

five with medium intensity (at  $(1549, 1549)$ ,  $(1266, 1266)$ ,  $(1003, 1003)$ ,  $(1011, 1011)$ , and  $(758, 758)$   $\text{cm}^{-1}$ ), and one with very weak intensity (at  $(1350, 1350)$   $\text{cm}^{-1}$ ). The strong intensity of the  $(1671, 1671)$   $\text{cm}^{-1}$  peak suggests that the enhancement of this SERS signal changed most significantly when the electrode potential became more negative. Several cross-peaks, both positive (at  $(1266, 1671)$ ,  $(1003, 1671)$ ,  $(758, 1671)$ ,  $(1011, 1549)$ ,  $(758, 1266)$ , and  $(758, 1003)$   $\text{cm}^{-1}$ ) and negative (at  $(1549, 1671)$ ,  $(1350, 1671)$ ,  $(1011, 1671)$ ,  $(1003, 1549)$ , and  $(1011, 1266)$   $\text{cm}^{-1}$ ), were also detected. These peaks correspond to the bands observed in the SERS spectra of NMC on Ag as previously discussed. A cross-peak with a positive sign indicates that the SERS signals involved increased in intensity with potential changes in the same direction. On the other hand, a negative sign means that the intensities of the signals changed in way opposite to that of the potential. Using these maps, we can conclude that the  $1671$ ,  $1266$ ,  $1003$ , and  $758$   $\text{cm}^{-1}$  SERS signals increased in relative intensity when the electrode potential became more negative, whereas the  $1350$ ,  $1549$ , and  $1011$   $\text{cm}^{-1}$  bands decreased in relative intensity.

Several cross-peaks were also observable in the asynchronous G2D correlation map (Figure 5A, right). The appearance of these peaks in the asynchronous spectrum suggests that the directions of the transition moments were different for each mode involved. The  $(758, 1549)$ ,  $(758, 1350)$ , and  $(758, 1011)$   $\text{cm}^{-1}$  cross-peaks had positive signs, indicating that potential-induced spectral changes took place at  $758$   $\text{cm}^{-1}$ , earlier than  $1549$ ,  $1350$ , or  $1011$   $\text{cm}^{-1}$ . On the other hand, the  $(1350, 1671)$ ,  $(1266, 1671)$ ,  $(1003, 1671)$ , and  $(758, 1671)$   $\text{cm}^{-1}$  cross-peaks had negative signs, which suggests that spectral alterations took place at  $1671$   $\text{cm}^{-1}$ , earlier than  $1350$ ,  $1266$ ,  $1003$ , and  $758$   $\text{cm}^{-1}$ . This information illustrates that the rearrangement of the amide bond on the Ag electrode surface initiated simultaneous changes in the orientation of Trp and His on this surface.

**Au Electrode Surface.** Almost all of the spectral features in the SERS spectra of NMC on the Au electrode surface (Figure 1B) could be correlated, without difficulty, to vibrations in the Trp, His, and  $-\text{CONH}-$  moieties. These include the SERS signals at  $758$ ,  $876$ ,  $1009$ ,  $1002$  (shoulder),  $1239$ ,  $1301$ ,  $1358$ ,  $1433$ ,  $1543$ ,  $1586$ , and  $1663$   $\text{cm}^{-1}$  (see Table 1 for band assignments) that closely correspond to the vibrational modes discussed earlier in the paper. Their wavenumber shifts ( $\Delta\nu = 0-8 \text{ cm}^{-1}$ ) and their width changes ( $\Delta_{\text{fwhm}} = 2-5 \text{ cm}^{-1}$ ) agree well with those reported for the Raman spectrum of NMC<sup>10</sup> and of NMC immobilized on the Ag electrode surface.<sup>9</sup> Therefore, we concluded that NMC indirectly interact with both the Ag and Au electrodes through Trp, His, and/or  $-\text{CONH}-$ . As mentioned earlier, the major differences in enhancement between the NMC SERS spectra on Au compared with spectra on Ag included stronger scattering at  $1358 \text{ cm}^{-1}$  ( $\nu(\text{N}_1-\text{C}_8)$ ) and weaker scattering at  $758$  and  $\sim 1009 \text{ cm}^{-1}$  on Au. These phenomena, together with moderate enhancement of the  $1301$ ,  $1433$ , and  $1543 \text{ cm}^{-1}$  SERS signals, indicate that the SERS enhancement was mainly produced by an interaction between the lone pair of electrons on the nitrogen atom and the electrode surface and by the interaction of  $\text{C}_8-\text{N}_1-\text{C}_2=\text{C}_3-\text{C}_9$  (the pyrrole coring) with the electrode surface. This may be supported by enhancement of the  $\nu(\text{C}_3-\text{C}_\beta\text{H}_2)$  ( $1239 \text{ cm}^{-1}$ ) band and of the aliphatic  $\nu(\text{C}_\alpha-\text{C}_\beta)$  of the Trp mode (at  $\sim 1117 \text{ cm}^{-1}$ ).

Careful analysis of the NMC SERS spectra on Au (Figure 1B) and of the G2D correlation maps (Figure 5B) generated from these spectra showed that marked variations in the relative intensities were observed for the  $1543$  and  $1358 \text{ cm}^{-1}$  spectral features when the electrode potential was changed, whereas at  $1433$ ,  $1298$ ,  $1009$ , and  $758 \text{ cm}^{-1}$ , only small changes in the enhancement were detected (Figure 5B, left). The positive signs of the cross-peaks, including the most prominent at  $(1358, 1543)$ ,  $(1009, 1543)$ ,  $(1009, 1358)$ ,  $(1301, 1543)$ , and  $(1301, 1358)$   $\text{cm}^{-1}$ , provide evidence that these SERS signals decreased in intensity with increasingly negative electrode potential. This in turn implies that there was only a small decrease in the indole ring tilt angle with respect to the Au surface and only a slight shift of the pyrrole-co ring from this surface. This inference may be additionally supported by the absence of the  $\nu(\text{C}_\alpha-\text{C}_\beta)_\text{Trp}$  mode in the NMC SERS spectrum at  $-1.200$  V. The lack of autopeaks due to vibrations of the amide bond ( $\sim 1269$  and  $\sim 1670 \text{ cm}^{-1}$ ) indicates that this structure is not affected by changes in the applied electrode potential on the Au electrode surface.

The asynchronous G2D correlation map (Figure 5B, right) depicts five prominent bands, four negative (at  $(1358, 1543)$ ,  $(1433, 1543)$ ,  $(758, 1543)$ , and  $(758, 1358)$   $\text{cm}^{-1}$ ) and one positive (at  $(1301, 1358)$   $\text{cm}^{-1}$ ). Along with a decrease in electrode potential from  $+0.200$  to  $-1.200$  V, the  $\text{C}_2=\text{C}_3-\text{C}_9 \cdots \text{Au}$  interactions weakened ( $I_{1543} \downarrow$  and  $I_{1301} \downarrow$ ), forcing a minor rearrangement of the indole ring surface. The pyrrole coring was pushed up slightly from the Au electrode and laid more parallel to this surface at  $-1.200$  V than at  $+0.200$  V. Hence, the  $1358$  and  $1433 \text{ cm}^{-1}$  spectral features and the  $758 \text{ cm}^{-1}$  band lost relative intensity. The indole W17 mode near  $877 \text{ cm}^{-1}$  was clearly visible in both the Au and Ag electrode SERS spectra (Figure 1 A and B). This mode was sensitive to changes in hydrogen bonding in the indole ring; the lower the frequency of the W17 mode, the stronger the hydrogen-bonding that occurs in the indole fragment of the tryptophane ring.<sup>37</sup> Compared with Ag at the same potential ( $878 \text{ cm}^{-1}$ ), the W17 band had a lower wavenumber ( $875 \text{ cm}^{-1}$ ) on the Au electrode at  $0.000$  V (Figure 1 B(b)). Thus, Figure

**TABLE 1: Wavenumbers and Proposed Band Assignments for Raman and SERS Spectra of NMC Adsorbed on Roughened Ag, Au, and Cu Electrode Surfaces<sup>a</sup>**

assignment	wavenumbers/cm <sup>-1</sup>					
	RS	Ag (0.000 V)	Au (0.200 V)	Cu (−0.800 V)	Ag, colloidal surface <sup>b</sup>	Ag, electrode surface <sup>c</sup>
AI $\beta$ -turn/antiparallel $\beta$ -sheet/unordered $\delta_{as}(NH_2)$	1671 1621	1671	1663	1668 (1639) <sup>d</sup>		
W2 [phenyl]and/or His <sub>N1-H</sub> [ $\nu(C=C)$ ]	<b>1579</b>	<b>1578</b>	<b>1586</b>	<b>1593 (1572)</b>		<b>1575</b>
W3 [pyrrole $\nu(C_2=C_3)$ ]	<b>1552</b>	<b>1549</b>		<b>1549 (1549)</b>	<b>1549</b>	<b>1544</b>
AII and/or W4 [benzene $\nu_{19b}$ ]						<b>1527</b>
W4 [benzene $\nu_{19b}$ , His [ring stretch + $\delta(N_1-H)$ ]	1492	1490		1491 (1481)		1483
W5 and $\rho_s(CH_2)$		1450	1443			
W6 [pyrrole ( $\nu_s(N_1C_2C_3) + \delta(N_1-H)$ ) + phenyl $\delta(CH)$ ], $\delta_{as}(CH_3)$ , and/or $\delta(CH_2)$	1433	1435	1433	1431 (1383)	1427	1438
$\nu_s(C=O)$ in pGlu, Asn, and/or Gln						1375
W7 [pyrrole ring $\nu(N_1-C_8)$ ; Fermi resonance], His, and/or $\rho_w(CH_2)$	<b>1361</b> <b>1340</b>	<b>1350</b>	<b>1358</b>	<b>1356 (1333)</b> <b>1340</b>	<b>1358</b> <b>1345</b>	
$\delta_{ip}(CH)$ , $\rho_t(CH_2)$ , W8 [ $\nu(C_3-C_9) + \delta(N_1-H)$ ], and/or His		1309	1301			1304
AIII and His [C—H in-plane bend/ring breathing]	1263	1264		1265 (1070)		
W10 [ $\nu(C_3-C_\beta H_2) + \nu(C-H)$ ] and His [CH in-plane bend/ring breathing]	<b>1236</b>	<b>1245</b>	<b>1239</b>		<b>1234</b>	
$\nu(C-C)_{Trp}$	1200				1182	1170
His[ $\delta(N_1-H)$ ]and/or $\rho_t(NH_2)$ in Asn		1170				
$\nu(C-C)_T$ alkyl chain	1127	1115	1117	1109 (1106)	1127	1110
$\nu(C-N)$ , $\rho_t(CH_2)$ , and/or His					1105	
$\nu(C-C)_T$ alkyl chain and/or $\rho_t(CH_2)$					1069	
W16 [phenyl and pyrrole out-of-phase ring breathing] and His [ring, C—H in-plane bend]	<b>1011</b>	<b>1011</b>	<b>1009</b>	<b>1010 (1011)</b>		
		1002				
$\nu(C-N)$ , $\rho_b(NH_2)$ , and/or benzene $\rho_b(CH)$						998
$\nu(C-C)$			956		950	
$\nu(C-C=O)$					928	
$\nu(C-C)$		903			908	
W17 [ $\delta(N_1-H)$ and Fermi resonance between phenyl ring breathing and oop ring bend overtone]	<b>877</b>	<b>878</b>	<b>876</b>	<b>878 (856)</b>	<b>878</b>	
$\nu(C-C)$					831	
$\nu(C-C)$ , $\nu_s(CNC)$ secondary amide, and/or His [ring oop bend]	835	830	834	831 (827)		809
$\nu(C-C)$					783	778
W18 [sym phenyl/pyrrole in-phase ring breathing]	<b>758</b>	<b>759</b>	<b>758</b>	<b>759 (754)</b>	<b>760</b>	<b>755</b>
W19	<b>724</b>		<b>734</b>			

<sup>a</sup> Abbreviations:  $\nu$  = stretching,  $\delta$  = deformation,  $\rho_w$  = wagging,  $\rho_b$  = bending,  $\rho_t$  = twisting, s = symmetric, as = antisymmetric, oop = out of plane, and ip = in plane vibrations. <sup>b</sup> According to ref 9. <sup>c</sup> According to ref 10. <sup>d</sup> Data from spectrum in D<sub>2</sub>O solution are presented in parentheses.

1A(a) illustrates a slight increase in the strength of the hydrogen bond interaction at the N<sub>1</sub>—H indole fragment for NMC adsorbed on the Au electrode surface. Interestingly, the wavenumber of this mode decreased with decreasing Ag electrode potentials, suggesting that the strength of the hydrogen bond interaction was potential dependent.

**Cu Electrode Surface.** A similar analysis can be made for NMC adsorbed on the Cu electrode (Figure 1C), and related conclusions can be drawn regarding interactions between the Cu surface and Trp residues, His residues, and amide bonds. In the SERS spectra on Cu, bands due to the C<sub>8</sub>—N<sub>1</sub>—C<sub>2</sub>=C<sub>3</sub>—C<sub>9</sub> coring and to the in-plane and out-of-plane indole ring vibrations (see Table 1 for the band positions) were relatively weakly enhanced, whereas the band at  $\sim 940\text{ cm}^{-1}$  due to phosphorus group vibrations was comparatively strong.<sup>38</sup> With this knowledge, a trend in competitive adsorption between the phosphonate ions and NMC can be observed in the NMC SERS spectral profiles on Cu. This behavior was distinctly different from the results obtained for this peptide immobilized on Ag and Au electrode surfaces, whereupon the band around  $940\text{ cm}^{-1}$  exhibited negligible enhancement. Also, the amide bond modes in the NMC SERS spectra were slightly enhanced on Cu compared with those on Ag and Au and were also slightly

enhanced compared to bands assignable to the Trp residue. In light of these observations, it is unlikely that the adsorption of NMC on Cu proceeded mainly through the —CONH— bond, which rested at an intermediate angle with respect to the Cu surface normal. Both the pyrrole and phenyl corings assisted in these interactions. On Cu, the synchronous G2D correlation map (Figure 5C, left) showed only one very strong autopeak at  $(940, 940)\text{ cm}^{-1}$  and two very weak autopeaks at  $(1593, 1593)$  and  $(1109, 1109)\text{ cm}^{-1}$ . The weak cross-peaks were assignable to the  $\nu(C_\alpha-C_\beta)_{Trp}$  and the phenyl coring vibrations (see Table 1 for assignment), respectively. This highlights the conclusion that only small orientation changes occurred in NMC on the Cu surface, and these mainly proceeded through the phenyl coring.

## Conclusions

Surface-enhanced Raman spectra (SERS) of adsorbed neuromedin C (NMC) on electrochemically roughened Ag, Au, and Cu electrode surfaces were dominated by characteristic L-tryptophan (Trp), L-histidine (His), and —CONH— vibrations over an electrode potential range varying from +0.200 to −1.200 V (varied depending on the electrode material). These

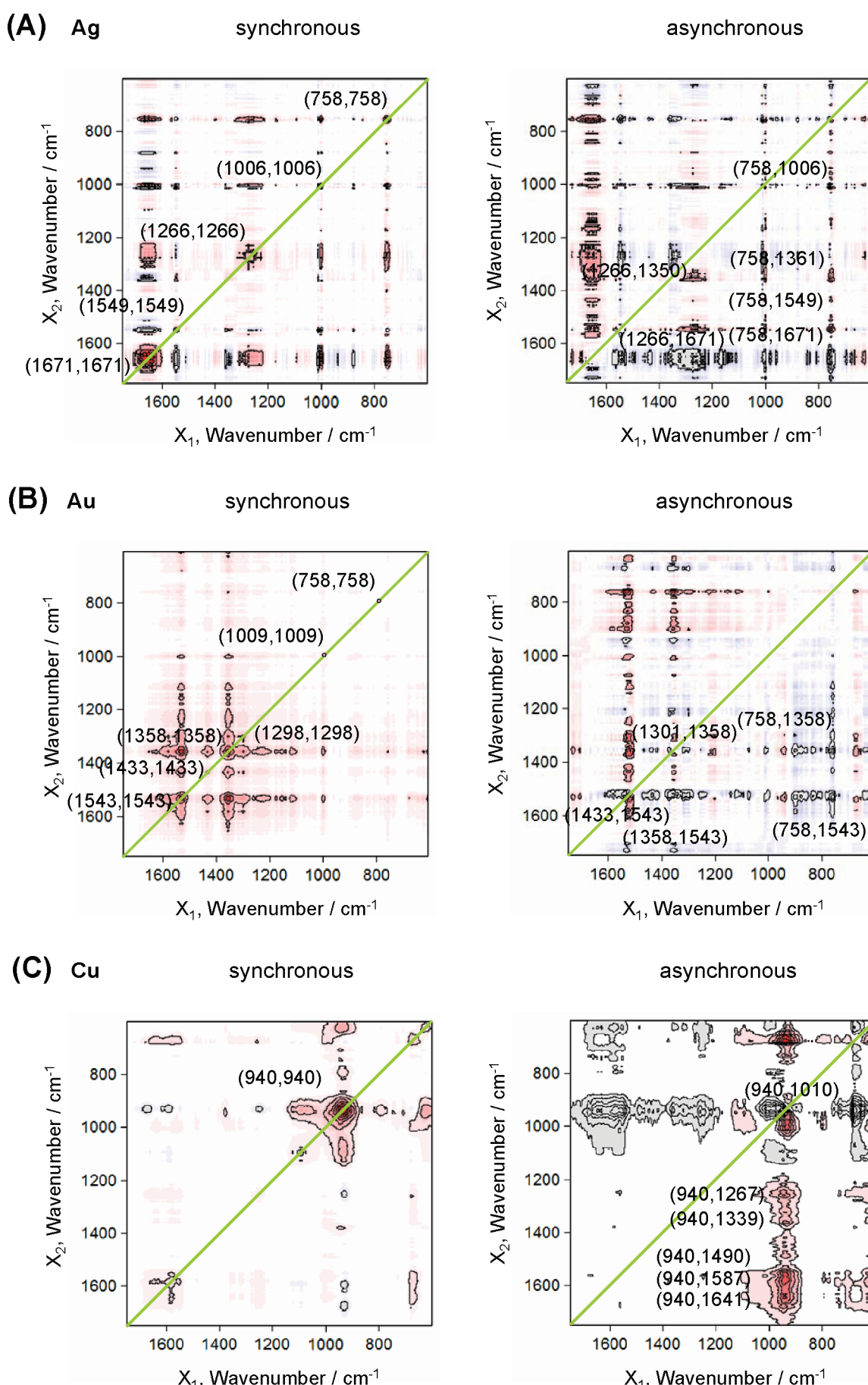


**Figure 5.** Generalized synchronous (left) and asynchronous (right) G2D correlation maps of the SERS spectra of NMC adsorbed on roughened (A) Ag, (B) Au, and (C) Cu electrodes as a function of electrode potential, within the spectral range 1750–600  $\text{cm}^{-1}$ .

data show that Trp and His interacted with the metallic electrode surface, either by binding directly to the surface or by remaining in close proximity to this surface. This finding agrees with the premise that Trp and His are the most active amino acids in NMC. As such, they play a crucial role in the binding of this decapeptide to its receptor. Characteristic SERS patterns show that, on an Ag electrode, the Trp residue adopted an almost perpendicular geometry with respect to the surface. In contrast, Trp was slightly tilted on a Au electrode surface, and it remained some distance from the surface of a Cu electrode. On the other hand, the imidazole ring in His adopted an orientation that was almost parallel to the Ag surface, while it was almost perpendicular to the Au and Cu surfaces (a possible manner of binding to the roughened Ag, Au, and Cu electrode surfaces of the His<sub>3</sub>—COOH—Trp<sub>4</sub> fragment of NMC is given in Figure 3). We showed that the rheology of the electrode surface, the applied potential, and the type of metal (Ag vs Au vs Cu) were all responsible for the observed differences in the SERS patterns. In general, such differences were due to modulation of the enhancement mechanism.

In addition, variations in electrode potentials had some influence on SERS band intensities and wavenumbers. In this work, observed changes were mainly due to the reorientation of the Trp and His rings with respect to the electrode surface. These findings were fully supported by generalized two-dimensional correlation analysis (G2DCA). We also suggest that the behavior of the W17 indole ring mode at 877 cm<sup>-1</sup> (representing δ(N<sub>1</sub>—H) coupled to the Fermi resonance between the phenyl ring breathing mode and the out-of-plane phenyl ring bending overtone) can serve as a hydrogen bond formation marker. On a Ag electrode, the wavenumber and intensity the W17 indole ring mode decreased with applied negative potential, indicating an increase in the strength of hydrogen bonding at the N<sub>1</sub>—H site of the indole ring. On the other hand, neither the wavenumber nor the intensity of this band changed upon NMC adsorption at the Au electrode. At more positive potential values (like 0.000 V), the hydrogen bond strength of NMC adsorbed on the Au electrode was stronger than in the case of Ag. Lastly, Trp and His vibrational bands assigned to the amide I and amide III modes were observed around 1670 and 1265 cm<sup>-1</sup>, respectively. This supports the formation of a β-structure of NMC adsorbed on the surfaces of roughened Ag, Au, and Cu electrodes.

**Acknowledgment.** This work was supported by the State Department for Scientific Research of the Ministry of Science and Higher Education (Grant No. N N204 159136 to E.P.).

**Supporting Information Available:** Reproducibility of the SERS results, Figure S1. This material is available free of charge via the Internet at <http://pubs.acs.org>.

## References and Notes

- (1) Lebacq-Verheyden, A. M.; Krystal, G.; Sartor, O.; Way, J.; Battey, J. F. *Mol. Endocrinol.* **1988**, 2, 556.
- (2) Reeve, J. R., Jr.; Walsh, J. H.; Chew, P.; Clark, B.; Hawke, D.; Shively, J. E. *J. Biol. Chem.* **1983**, 258, 5582.
- (3) Spindel, E. R.; Chin, W. W.; Price, J.; Rees, L. H.; Besser, G. M.; Habener, J. F. *Proc. Natl. Acad. Sci. U.S.A.* **1984**, 81, 5699.
- (4) Bunnet N. Gastrin releasing peptide. In *Gut Peptides: Biochemistry and Physiology*; Walsh, J. H., Dockray, G. J., Eds.; Raven Press: New York, 1994; p 423.
- (5) Dumesny, Ch.; Whitley, J. C.; Baldwin, G. S.; Giraud, A. S.; Shulkes, A. *Am. J. Physiol. Renal Physiol.* **2004**, 287, F578.
- (6) Otsuki, M.; Fujii, M.; Nakamura, T.; Tani, S.; Oka, T.; Yajima, H.; Baba, S. *Am. J. Physiol.* **1987**, 252, G491.
- (7) Spindel, E. R.; Giladi, E.; Brehm, P.; Goodman, R. H.; Segerson, T. P. *Mol. Endocrinol.* **1990**, 4, 1956.
- (8) Bunnet, G. In *Gastrin-releasing peptide*, in *Gut peptides: biochemistry and physiology*; Walsh, J. H., Dockray, G. J., Eds.; Raven Press: New York, 1994; p 423.
- (9) Podstawka, E.; Proniewicz, L. M. *J. Phys. Chem. B* **2009**, 113, 4978.
- (10) Podstawka, E. *Biopolymers* **2008**, 89, 980.
- (11) Lewis, I. R., Edwards, H. G. M., Eds. *Handbook Of Raman Spectroscopy. Practical Spectroscopy*; Marcel Dekker, Inc.: New York, 2001.
- (12) Vo-Dinh, T.; Yan, F.; Wabuyele, M. B. *J. Raman Spectrosc.* **2005**, 36, 640.
- (13) Baena, J. R.; Lendl, B. *Curr. Opin. Chem. Biol.* **2004**, 8, 534.
- (14) Podstawka, E.; Olszewski, T. K.; Boduszek, B.; Proniewicz, L. M. *J. Phys. Chem. B* **2009**, 113, 12013.
- (15) Pelletier, M. J. *Analytical applications of Raman spectroscopy*; Blackwell Publishing: Edinburgh, 1999.
- (16) Ryder, A. G. *Curr. Opinion Chem. Biol.* **2005**, 9, 489.
- (17) Etchegoin, P. G.; Maher, R. C.; Cohen, L. F.; Hartigan, H.; Brown, R. J. C.; Milton, M. J. T.; Gallop, J. C. *Chem. Phys. Lett.* **2003**, 375, 84.
- (18) Kneipp, K.; Moskovits, M.; Kneipp, H. *Surface-Enhanced Raman Scattering: Physics And Applications*; Springer-Verlag: Berlin, 2006.
- (19) Niaura, G.; Gaigalas, A. K.; Vilker, V. L. *J. Raman Spectrosc.* **1997**, 28, 1009.
- (20) Bulovas, A.; Dirvianskytė, N.; Talaikytė, Z.; Niaura, G.; Valentukonytė, S.; Butkus, E.; Razumas, V. *J. Electroanal. Chem.* **2006**, 591, 175.
- (21) Kazakevičienė, B.; Valincius, G.; Niaura, G.; Talaikytė, Z.; Kažemėkaitė, M.; Razumas, V. *J. Phys. Chem. B* **2003**, 107, 6661.
- (22) Gao, P.; Gosztola, D.; Leung, L. W. H.; Weaver, M. J. *J. Electroanal. Chem.* **1987**, 233, 211.
- (23) Roth, E.; Hope, G. A.; Scheweinsberg, D. P.; Kiefer, W.; Fredericks, P. M. *Appl. Spectrosc.* **1993**, 47, 1794.
- (24) Niaura, G.; Malinauskas, A. *Chem. Phys. Lett.* **1993**, 207, 455.
- (25) Kneipp, K.; Kneipp, H.; Itzkan, I.; Dasari, R. R.; Feld, M. S. *Chem. Rev.* **1999**, 99, 2957.
- (26) Podstawka, E.; Niaura, G. *J. Phys. Chem. B* **2009**, 113, 10974.
- (27) Podstawka, E.; Ozaki, Y.; Proniewicz, L. M. *Langmuir* **2008**, 24, 10807.
- (28) Podstawka, E.; Ozaki, Y. *Biopolymers* **2008**, 89, 941.
- (29) Podstawka, E.; Ozaki, Y. *Biopolymers* **2008**, 89, 807.
- (30) Podstawka, E. *Biopolymers* **2008**, 89, 506.
- (31) Podstawka, E. *J. Raman Spectrosc.* **2008**, 39, 1290.
- (32) Podstawka, E.; Niaura, G.; Proniewicz, L. M. *J. Phys. Chem. B* **2009**, 114, 1010.
- (33) Martusevičius, S.; Niaura, G.; Talaikytė, Z.; Razumas, V. *Vibr. Spectrosc.* **1996**, 10, 271.
- (34) Lim, J. K.; Kim, Y.; Lee, S. Y.; Joo, S. W. *Spectrochim. Acta A* **2008**, 69, 286.
- (35) Carter, D. A.; Pemberton, J. E. *Langmuir* **1992**, 8, 1218.
- (36) Jung, J. M.; Kim, S. B. *J. Korean Phys. Soc.* **2004**, 45, 652.
- (37) Takeuchi, H. *Biopolymers* **2003**, 72, 305.
- (38) Niaura, G.; Gaigalas, A. K.; Vilker, V. L. *J. Phys. Chem. B* **1997**, 101, 9250.